IEEE Access
Multidisciplinary | Rapid Review | Open Access Journal

Received May 27, 2020, accepted June 3, 2020, date of publication June 8, 2020, date of current version June 17, 2020.

Digital Object Identifier 10.1109/ACCESS.2020.3000763

Automated Cone Photoreceptor Cell Segmentation and Identification in Adaptive Optics Scanning Laser Ophthalmoscope Images Using Morphological Processing and Watershed Algorithm

YIWEI CHEN[1], YI HE[1], JING WANG[1,2], WANYUE LI[1,2], LINA XING[1], FENG GAO[1], AND GUOHUA SHI[1,2,3]

[1]Jiangsu Key Laboratory of Medical Optics, Suzhou Institute of Biomedical Engineering and Technology, Chinese Academy of Sciences, Suzhou 215163, China
[2]Department of Biomedical Engineering, University of Science and Technology of China, Hefei 230041, China
[3]Center for Excellence in Brain Science and Intelligence Technology, Chinese Academy of Sciences, Shanghai 200031, China

Corresponding author: Guohua Shi (ghshi_lab@126.com)

This work was supported in part by the Jiangsu Province Key Research and Development Program under Grant BE2019682 and Grant BE2018667, in part by the National Natural Science Foundation of China under Grant 61605210, Grant 61675226, and Grant 61378090, in part by the Youth Innovation Promotion Association of Chinese Academy of Sciences under Grant 2019320, in part by the National Key Research and Development Program of China under Grant 2016YFC0102500 and Grant 2017YFB0403700, in part by the Frontier Science Research Project of the Chinese Academy of Sciences under Grant QYZDB-SSW-JSC03, and in part by the Strategic Priority Research Program of the Chinese Academy of Sciences under Grant XDB02060000.

ABSTRACT Geometrical analysis of cone photoreceptor cells is important not only for ophthalmic diagnosis, but also for research on eye diseases. In this study, an automated cone photoreceptor cell segmentation and identification method based on morphological processing and watershed algorithm is presented for adaptive optics scanning laser ophthalmoscope images. Our method includes steps for image denoising, rough segmentation, fine segmentation, small region removal, and identification. The effectiveness of the proposed method was confirmed by comparing its results with those obtained manually yielding precision, recall, and F1-score values of 93.6%, 98.0% and 95.8%, respectively. The performance of our method is further verified by processing images with different cone photoreceptor cell densities from healthy retina and an image from an eye with diabetic retinopathy. The experimental results show that our algorithm achieved high accuracy in cone photoreceptor cell segmentation and identification in healthy retinas as well as in retina with diabetic retinopathy.

INDEX TERMS Retinal images, adaptive optics scanning laser ophthalmoscope, image segmentation.

I. INTRODUCTION

Adaptive optics (AO) involves improving resolutions of optical instruments by correcting optical aberrations; this technology was originally used to eliminate the effects of atmospheric distortion in astronomical telescopes [1] and was subsequently introduced in retinal imaging to correct ocular aberrations [2]–[8]. As an AO integrated instrument, the adaptive optics scanning laser ophthalmoscope (AO-SLO) can be used to perform *in vivo* retinal imaging at a cellular level [4], [9]–[11]. Accordingly, AO-SLO images can be used for segmentation and identification of cone photoreceptor cells, which would be of significant importance not only for understanding the cellular nature of retinal diseases, thus improving their prognosis and diagnosis, but also for the study of ophthalmic treatment efficacy and examination. Although manual methods for segmentation and identification of cone photoreceptor cells are accurate and reliable, the associated labor costs and time required to perform them are excessive. Therefore, several studies aimed at the development of semi-automated and automated methods for segmentation and identification of cone

The associate editor coordinating the review of this manuscript and approving it for publication was Shiping Wen.

photoreceptor cells have been conducted; these methods include non-learning [12]–[16], supervised-learning-[17]–[19], and unsupervised-learning-based methods [20]. Although these methods achieve high accuracy in cone photoreceptor cell segmentation and identification in healthy retinas, there is no study that confirms the high accuracy of the existing methods for all types of eye diseases. In fact, it was reported that the existing methods achieve high accuracy in cone photoreceptor cell segmentation and identification in subjects with Stargardt disease [19], [20] and achromatopsia [17]. The major challenge encountered in cone photoreceptor cell segmentation and identification in subjects with pathological eyes is that the distribution and appearance of the photoreceptor cells differ from those in subjects with healthy eyes. Therefore, after performing automated cone photoreceptor cell segmentation and identification, the errors in the results are manually corrected and high accuracy is achieved for some cases. To automatically segment and identify cone photoreceptor cells in every type of pathological eye with high accuracy, there is a need for a new method to be developed. One efficient way is to use existing methods that have not yet been applied in the domain of cone photoreceptor cell segmentation and identification in AO-SLO but are known for their high accuracy in image segmentation and identification, or to combine them.

Herein, we propose a new combination of morphological processing and watershed algorithm to both segment and identify cone photoreceptor cells in AO-SLO images to achieve good performance not only for healthy eyes but also for eyes with diabetic retinopathy. To confirm the effectiveness of our proposed method, we compared our identification results with those obtained manually in terms of precision, recall, and F1-score. To further demonstrate the performance of our method, the cone photoreceptor cell segmentation and identification results for images with different cone photoreceptor cells densities from healthy retinae as well as for an image of a pathological eye with diabetic retinopathy obtained using our proposed approach are presented.

II. METHODS

In this section, our proposed automated image processing method for segmentation and identification of cone photoreceptor cells is described. The flowchart for the proposed image processing algorithm is shown in Fig. 1. It includes five steps, namely image denoising, rough segmentation, fine segmentation, small region removal, and cells identification. First, an AO-SLO image is denoised by averaging multiple registered images [21]. Second, the cone photoreceptor cells were roughly segmented via adaptive threshold segmentation and global morphological processing. Third, fine segmentation was performed using local morphological processing and watershed algorithm to further remove the conjunctions between cone photoreceptor cells in the obtained rough segmentation results. Fourth, segmented regions with areas smaller than a threshold were removed to exclude regions that do not contain cone photoreceptor cells. Finally, cone photoreceptor cells were identified as the centroids of cone photoreceptor cell-containing regions.

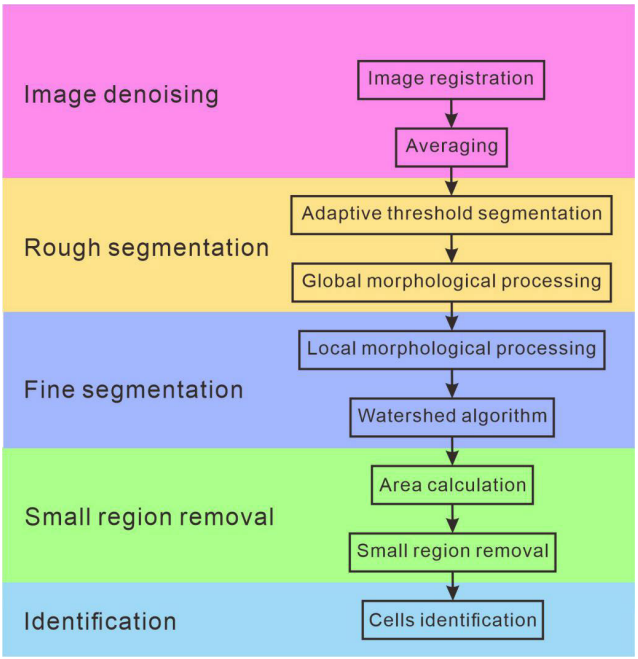

FIGURE 1. Flowchart of our automated image processing method for the segmentation and identification of cone photoreceptor cells.

A. IMAGE DENOISING

Owing to the limited light exposure resilience of the human eye, to ensure safety, the power of the AO-SLO imaging light is low, which results in a low signal-to-noise ratio (SNR) in AO-SLO images. To enhance the SNR in AO-SLO images, we averaged multiple AO-SLO images that were registered using the optical flow-based registration method [21]; in particular, this registration method can be used to perform accurate registration owing to its property of high number of registration degrees of freedom [21]. An example of image denoising on a representative image patch performed using this method is shown in Fig. 2. As shown in the figure, the noise in the image was significantly suppressed after denoising was performed, which confirms the effectiveness of the denoising method presented in [21]. To achieve fine segmentation of cone photoreceptor cells, we magnified the denoised image five times isotropically via bicubic interpolation after image denoising and before segmentation.

B. ROUGH SEGMENTATION

1) ADAPTIVE THRESHOLD SEGMENTATION

As the initial segmentation approach for cone photoreceptor cells, we applied adaptive threshold segmentation using OpenCV's adaptiveThreshold function in Python with a mean-value-based threshold. Compared with unified threshold segmentation, the adaptive threshold segmentation approach can be used to segment cone photoreceptor cells in an image adaptively based on the differences in image

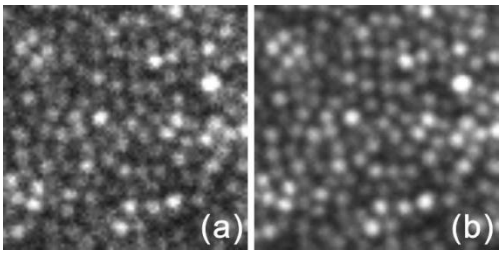

FIGURE 2. Example of image denoising using the optical flow-based image registration method: (a) Image before denoising, and (b) image after denoising.

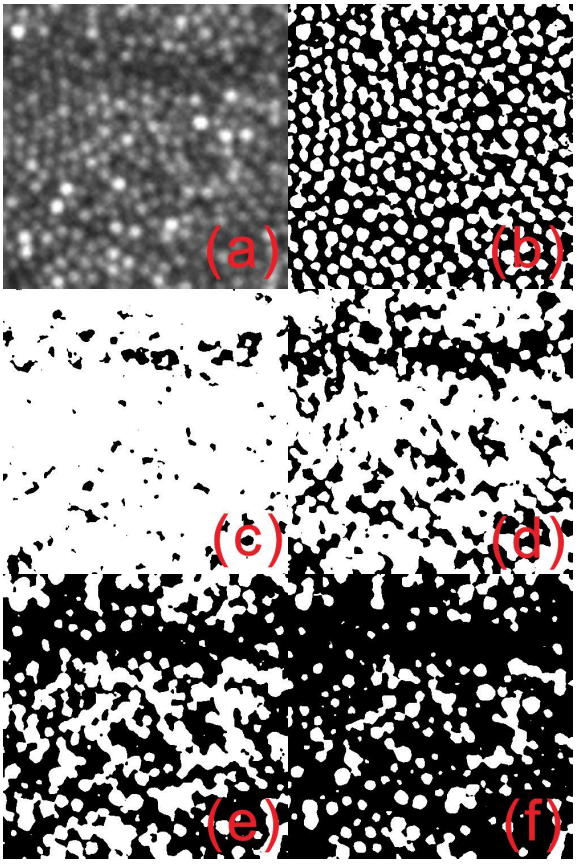

FIGURE 3. Comparison of adaptive threshold segmentation with unified threshold segmentation approaches. (a) Input image. (b) Adaptive threshold segmentation results on image, and (c–f) unified threshold segmentation results with intensity thresholds of 60, 80, 100, and 120, respectively.

intensities in the image. To demonstrate the much better segmentation performance of the adaptive threshold segmentation approach than unified threshold segmentation which is simpler, we compared segmentation results obtained using it with those obtained using four different unified threshold segmentation approaches; these results are shown in Fig. 3. As shown in the figure, the adaptive threshold segmentation approach yielded much better results (Fig. 3(b)) than the unified threshold segmentation approaches, which all failed to simultaneously segment the dark and bright cone photoreceptor cells (Figs. 3(c)–(f)).

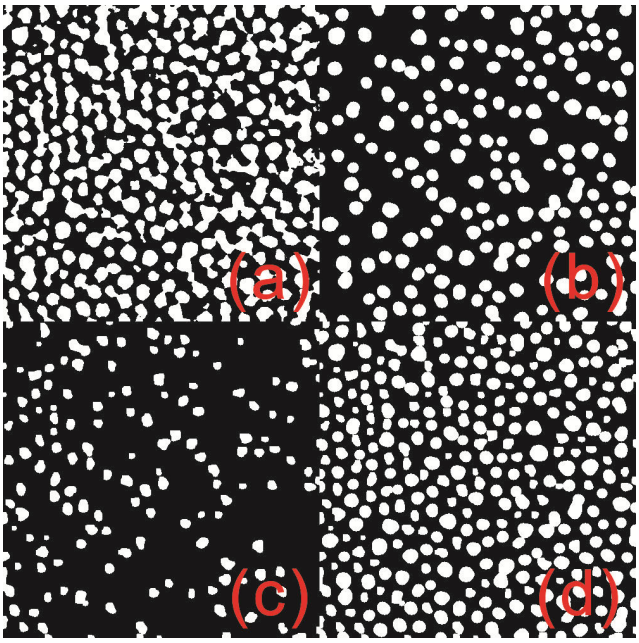

FIGURE 4. Example of global morphological processing. (a) Adaptive threshold segmentation results as input, (b) large segmented regions, (c) small segmented regions, and (d) final combined results of global morphological processing.

2) GLOBAL MORPHOLOGICAL PROCESSING

To further segment the entire cone photoreceptor cells image after adaptive threshold segmentation, we performed global morphological processing on the adaptive threshold segmentation results. First, morphological opening operation was applied to adaptive threshold segmentation results to obtain large segmented regions. Second, morphological top-hat operation is applied to the adaptive threshold segmentation results and then the morphological opening operation is applied to the top-hat operation results to obtain small segmented regions. Finally, the large and small segmented regions were combined together to obtain the final global morphological processing results. An example of global morphological processing using a representative image patch—the same as that used in Fig. 3—is shown in Fig. 4.

C. FINE SEGMENTATION

1) LOCAL MORPHOLOGICAL PROCESSING

Despite performing rough segmentation, there is a high probability that some cone photoreceptor cells still appear conjoined with other cone photoreceptor cells in the rough segmentation results. To partially address this problem, we apply local morphological processing on the rough segmentation results to segment regions containing conjunctions between cone photoreceptor cells. First, regions whose contours lengths were longer than the threshold of one cone photoreceptor cell contour-length were regarded as regions containing conjunctions. Second, the minimum enclosing rectangles for each conjunction-containing region were cropped. Third, morphological processing was applied on each rectangle; here, the algorithm for morphological

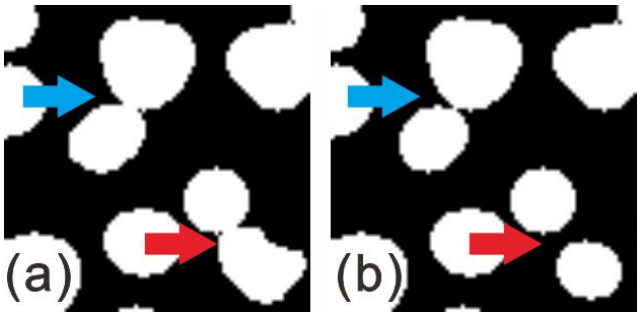

FIGURE 5. Example of local morphological processing. (a) Segmentation results before local morphological processing, and (b) after processing. The red arrow indicates a successful segmentation, while the blue arrow indicates an unsuccessful segmentation.

processing is the same as that of global morphological processing, which combines the morphological opening operation processed results and morphological top-hat operation processed results, albeit with different parameters. Finally, the rough segmentation results are updated with the morphological processing results obtained for the enclosing rectangles. An example of local morphological processing using a representative image patch is shown in Fig. 5. As shown in the figure, the conjunction-containing regions may (red arrow) or may not (blue arrow) be segmented.

2) WATERSHED ALGORITHM

After local morphological processing, conjunction-containing regions could still be present in the segmentation results. To solve this problem, we apply the watershed algorithm to the local morphological processing results. First, we used the same method to determine conjunction-containing regions, which detect those regions by the threshold of the contour-length of one cone photoreceptor cell, and crop rectangles for each of them as in the local morphological processing step. Second, we applied marker-controlled watershed segmentation to each rectangle using OpenCV's watershed function in Python. As inputs for the marker-controlled watershed segmentation method, markers of objects, background, and unknown areas are required. Accordingly, the markers of objects were obtained via threshold-based segmentation as follows:

$$\text{Object Area} = \{\text{Location} \mid \text{Intensity(Location)} \geq \text{Threshold}\} \tag{1}$$

where

$$\text{Threshold} = \min(\text{Bright}) + [\max(\text{Bright}) - \min(\text{Bright})] \times \text{Rate} \tag{2}$$

$$\text{Bright} = \{\text{Intensity} \mid \text{Intensity} \geq \text{mean(Intensities)}\} \tag{3}$$

In (2) and (3), "Bright" refers the bright part of an AO-SLO image, while "Rate" is a value between 0 and 1. Furthermore, the markers for the background were set to be the same as local morphological processing results, while the remainder of the area was set as markers for unknown area. The marker-controlled watershed segmentation method was applied iteratively with an increasing rate until no conjunction-containing regions are detected using the previously discussed contour-length threshold-based method. After these iterations, the contour-length of each region is smaller than the threshold of the contour-length of one cone photoreceptor cell, thereby avoiding the conjunction-containing regions. Finally, the local morphological processing results are updated with all marker-controlled watershed segmented rectangles. As an example, the results of the watershed algorithm applied to a representative image patch are shown in Fig. 6; as shown in the figure, the conjunction-containing regions are clearly segmented (see red arrows).

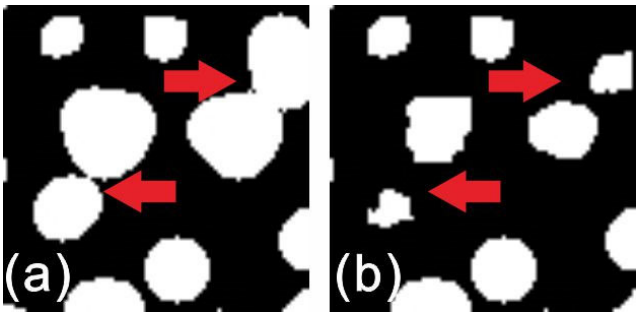

FIGURE 6. Watershed algorithm results for an example image patch (a) before processing, and (b) after processing. Red arrows indicate two successful segmentations.

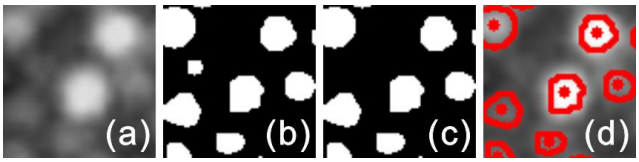

FIGURE 7. Example of small region removal and cells identification. (a) Denoised AO-SLO image (b) before small region removal, and (c) after small region removal. (d) Final results of cell segmentation and identification.

D. SMALL REGION REMOVAL AND CELLS IDENTIFICATION

Even after conducting the segmentation processing described above, some regions without cells are still present owing to different reasons, such as residual noise. The areas of regions that do not contain cells are typically smaller the regions containing cells. Thus, regions whose areas are smaller than 20% of the largest region are removed from consideration. After this removal, the remaining regions are regarded as our final cone photoreceptor cells image segmentation results; these results are then used for cells identification, which is performed by calculating the centroid of each region in the final segmentation results. An example of small region removal and cells identification using a representative image patch is shown in Fig. 7. As shown in the figure, the regions without cells were removed after small region removal; the final cell segmentation and identification results are shown in Fig. 7(d).

TABLE 1. Comparison of the Performance Metrics for Cell Identification: Overall Precision, Recall, and F1-Score Outcomes.

	State-of-the-art Algorithm [Reference 12]	Our Algorithm
Precision	94.7%	93.6%
Recall	99.4%	98.0%
F1-score	97.0%	95.8%

III. RESULTS

An AO-SLO with an imaging rate of 30 Hz was used for imaging the posterior parts of human eyes. The field-of-view (FOV) on the human retina is 1.5° and the corresponding frame size is approximately 512 × 449 pixels. Thus, a transverse area of approximately 445 μm × 445 μm was scanned based on the assumption of a focal length of 17 mm for the human eye. The details of the AO-SLO system are described in [22]. Drops of tropicamide (1%) and phenylephrine hydrochloride (2.5%) were administered to dilate the pupil to a diameter in the range of 6–8 mm before imaging. Light exposure adhered to the maximum permissible exposure limits set by the American National Standards Institute [23] throughout the procedure.

The typical computational times for processing a 100 × 100 image using our automated approach are as follows: 49.71 s for image denoising, 0.0020 s for adaptive threshold segmentation, 0.0069 s for global morphological processing, 0.0259 s for local morphological processing, 0.0189 s for the application of the watershed algorithm, 0.0199 s for small region removal, and 0.0050 s for cells identification. These computational times were obtained using a system with an Intel Core i5-9400 CPU operating at 2.90 GHz, NVIDIA GeForce GTX 1660 Ti graphic card, and 16.0 GB RAM. The image denoising program was written in MATLAB (64-bit) and CUDA 10.0, while the other programs were written in Python (64-bit).

To evaluate the effectiveness of our method, images of five eyes from five healthy subjects were obtained near the centers of their foveae. Our method successfully segmented and identified cone photoreceptor cells in the five eye datasets, and three typical results are shown in Fig. 8. The overall precision, recall, and F1-score for identification are listed in Table 1 and the values are compared with those of the state-of-the-art algorithm [12]; here, manual identification of cone photoreceptor cells is considered as the ground truth. Based on the performance results, it is clear that our algorithm achieves high accuracy for identification of cone photoreceptor cells, which is very approaching to the state-of-the-art algorithm [12] near the centers of foveae from healthy subjects.

To test the performance of our method for different types of images, three examples with input AO-SLO images (Figure 9a), corresponding segmented images (Figure 9b), and corresponding identification results (Figure 9c) are presented in Figure 9. The first and second examples were images from different locations of a healthy retina whose cone photoreceptor cells density is smaller than examples in Fig. 8 (shown in the top two rows in Figure 9). The bottom row in Fig. 9 shows an example of an AO-SLO image of an eye with diabetic retinopathy [24] along with the corresponding segmentation and identification results. Based on the examples show in Figure 9, it is clear that our algorithm also provided accurate segmentation results for images with smaller cone photoreceptor cells density as well as diabetic retinopathy.

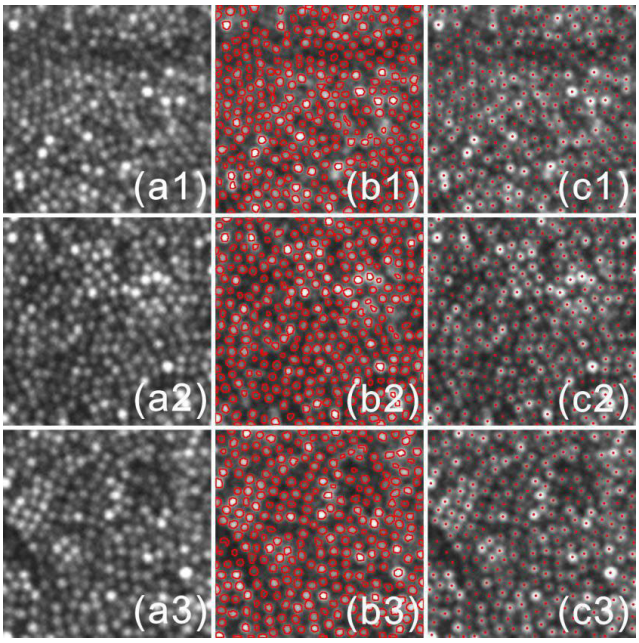

FIGURE 8. Typical segmentation results obtained using the proposed method. (a) Input AO-SLO images. (b) Segmentation of cells in the images. (c) Identification of cells in the images.

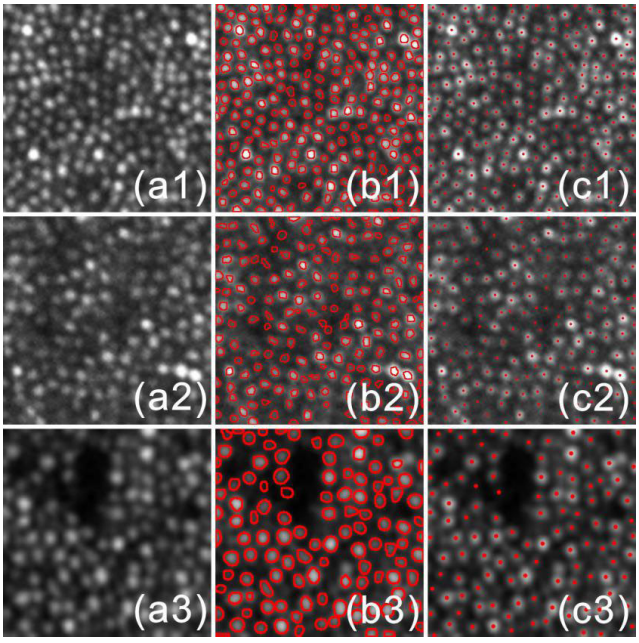

FIGURE 9. Performance of the proposed method. (a) Input AO-SLO images. (b) Segmentation of cells in the images. (c) Identification of cells in the images.

IV. DISCUSSION

As mentioned earlier, an efficient way to enable automatic segmentation and identification of cone photoreceptor cells in every type of pathological eye is to use methods that have not yet been applied in cone photoreceptor cell segmentation and identification in AO-SLO, but are known for their high accuracy in image segmentation and identification, or their combinations. In this regard, we presented the modified versions of three famous methods [25]–[27] as promising solutions for dealing with some types of eye diseases.

V. CONCLUSIONS

In this study, an automated method for segmentation and identification of cone photoreceptor cells was proposed. Morphological processing and watershed algorithm were primary approaches used in our method for segmentation and identification of cone photoreceptor cells in AO-SLO images. The effectiveness of our proposed approach was confirmed based on the results of adaptive threshold segmentation, global morphological processing, local morphological processing, watershed algorithm, small region removal, and cells identification. To further confirm the performance of our proposed method, we compared the cone photoreceptor cells identification results with those of manual identification and obtained precision, recall, and F1-score metrics of 93.6%, 98.0%, and 95.8% for cells identification, respectively, which is very approaching to the ones of state-of-the-art algorithm [12] near the centers of foveae from healthy subjects. In addition, the performance of our method was also demonstrated for different types of images, including those with smaller cone photoreceptor cells densities and diabetic retinopathy. The experimental results show that our algorithm can achieve high accuracy in cone photoreceptor cell segmentation and identification in healthy retinas as well as in retina with diabetic retinopathy. Our proposed method would be helpful for standard ophthalmic examinations as well as the geometrical analysis of cone photoreceptor cells.

ACKNOWLEDGMENT

The authors wish to thank the anonymous reviewers for their valuable suggestions.

REFERENCES

[1] H. W. Babcock, "The possibility of compensating astronomical seeing," *Publ. Astronomical Soc. Pac.*, vol. 65, no. 386, pp. 229–236, 1953.

[2] A. Roorda, F. Romero-Borja, W. J. Donnelly, III, H. Queener, T. J. W. Hebert, and M. C. Campbell, "Adaptive optics scanning laser ophthalmoscopy," *Opt. Express*, vol. 10, pp. 405–412, May 2002.

[3] S. A. Burns, R. Tumbar, A. E. Elsner, D. Ferguson, and D. X. Hammer, "Large-field-of-view, modular, stabilized, adaptive-optics-based scanning laser ophthalmoscope," *J. Opt. Soc. Amer. A, Opt. Image Sci.*, vol. 24, no. 5, pp. 1313–1326, 2007.

[4] R. D. Ferguson, Z. Zhong, D. X. Hammer, M. Mujat, A. H. Patel, C. Deng, W. Zou, and S. A. Burns, "Adaptive optics scanning laser ophthalmoscope with integrated wide-field retinal imaging and tracking," *J. Opt. Soc. Amer. A, Opt. Image Sci.*, vol. 27, no. 11, pp. A265–A277, 2010.

[5] A. Dubra and Y. Sulai, "Reflective afocal broadband adaptive optics scanning ophthalmoscope," *Biomed. Opt. Express*, vol. 2, no. 6, pp. 1757–1768, 2011.

[6] N. D. Shemonski, F. A. South, Y.-Z. Liu, S. G. Adie, P. S. Carney, and S. A. Boppart, "Computational high-resolution optical imaging of the living human retina," *Nature Photon.*, vol. 9, no. 7, pp. 440–443, Jul. 2015.

[7] J. Lu, B. Gu, X. Wang, and Y. Zhang, "High speed adaptive optics ophthalmoscopy with an anamorphic point spread function," *Opt. Express*, vol. 26, no. 11, pp. 14356–14374, 2018.

[8] S. Mozaffari, V. Jaedicke, F. Larocca, P. Tiruveedhula, and A. Roorda, "Versatile multi-detector scheme for adaptive optics scanning laser ophthalmoscopy," *Biomed. Opt. Express*, vol. 9, no. 11, pp. 5477–5488, 2018.

[9] A. W. Dreher, J. F. Bille, and R. N. Weinreb, "Active optical depth resolution improvement of the laser tomographic scanner," *Appl. Opt.*, vol. 28, no. 4, pp. 804–808, 1989.

[10] J. Liang, D. R. Williams, and D. T. Miller, "Supernormal vision and high-resolution retinal imaging through adaptive optics," *J. Opt. Soc. Amer. A, Opt. Image Sci.*, vol. 14, pp. 2884–2892, Nov. 1997.

[11] H. Hofer, L. Chen, G. Y. Yoon, B. Singer, Y. Yamauchi, and D. R. Williams, "Improvement in retinal image quality with dynamic correction of the eye's aberrations," *Opt. Express*, vol. 8, no. 11, pp. 631–643, 2001.

[12] K. Y. Li and A. Roorda, "Automated identification of cone photoreceptors in adaptive optics retinal images," *J. Opt. Soc. Amer. A, Opt. Image Sci.*, vol. 24, no. 5, pp. 1358–1363, 2007.

[13] A. Turpin, P. Morrow, B. Scotney, R. Anderson, and C. Wolsley, "Automated identification of photoreceptor cones using multi-scale modelling and normalized cross-correlation," in *Proc. Int. Conf. Image Anal. Process.*, Berlin, Germany: Springer, 2011, pp. 494–503.

[14] S. J. Chiu, Y. Lokhnygina, A. M. Dubis, A. Dubra, J. Carroll, J. A. Izatt, and S. Farsiu, "Automatic cone photoreceptor segmentation using graph theory and dynamic programming," *Biomed. Opt. Express*, vol. 4, no. 6, pp. 924–937, 2013.

[15] D. M. Bukowska, A. L. Chew, E. Huynh, I. Kashani, S. L. Wan, P. M. Wan, and F. K. Chen, "Semi-automated identification of cones in the human retina using circle Hough transform," *Biomed. Opt. Express*, vol. 6, no. 12, pp. 4676–4693, 2015.

[16] J. Liu, H. Jung, A. Dubra, and J. Tam, "Automated photoreceptor cell identification on nonconfocal adaptive optics images using multiscale circular voting," *Invest. Ophthalmol. Vis. Sci.*, vol. 58, no. 11, pp. 4477–4489, 2017.

[17] D. Cunefare, C. S. Langlo, E. J. Patterson, S. Blau, A. Dubra, J. Carroll, and S. Farsiu, "Deep learning based detection of cone photoreceptors with multimodal adaptive optics scanning light ophthalmoscope images of achromatopsia," *Biomed. Opt. Express*, vol. 9, no. 8, pp. 3740–3756, 2018.

[18] D. Cunefare, L. Fang, R. F. Cooper, A. Dubra, J. Carroll, and S. Farsiu, "Open source software for automatic detection of cone photoreceptors in adaptive optics ophthalmoscopy using convolutional neural networks," *Sci. Rep.*, vol. 7, no. 1, pp. 1–11, Dec. 2017.

[19] B. Davidson, A. Kalitzeos, J. Carroll, A. Dubra, S. Ourselin, M. Michaelides, and C. Bergeles, "Automatic cone photoreceptor localisation in healthy and stargardt afflicted retinas using deep learning," *Sci. Rep.*, vol. 8, no. 1, pp. 1–13, Dec. 2018.

[20] C. Bergeles, A. M. Dubis, B. Davidson, M. Kasilian, A. Kalitzeos, J. Caroll, A. Dubra, M. Michaelides, and S. Ourselin, "Unsupervised identification of cone photoreceptors in non-confocal adaptive optics scanning light ophthalmoscope images," *Biomed. Opt. Express*, vol. 8, no. 6, pp. 3081–3094, 2017.

[21] Y. Chen, Y. He, J. Wang, W. Li, L. Xing, F. Gao, and G. Shi, "Automated optical flow based registration for adaptive optics scanning laser ophthalmoscope," *IEEE Photon. J.*, vol. 12, no. 2, pp. 1–9, Apr. 2020.

[22] Y. Wang, Y. He, L. Wei, X. Li, J. Yang, H. Zhou, and Y. Zhang, "Bimorph deformable mirror based adaptive optics scanning laser ophthalmoscope for retina imaging *in vivo*," *Chin. Opt. Lett.*, vol. 15, no. 12, 2017, Art. no. 121102.

[23] *American National Standard for Safe Use of Lasers*, A. N. S. Inst., Laser Inst. Amer., Orlando, FL, USA, 2007.

[24] S. A. Burns, A. E. Elsner, K. A. Sapoznik, R. L. Warner, and T. J. Gast, "Adaptive optics imaging of the human retina," *Prog. Retin. Eye Res.*, vol. 68, pp. 1–30, Jan. 2019.

[25] S. Wen, W. Liu, Y. Yang, and T. Huang, "Generating realistic videos from keyframes with concatenated GANs," *IEEE Trans. Circuits Syst. Video Technol.*, vol. 29, no. 8, pp. 2337–2348, Aug. 2019.

[26] M. Dong, S. Wen, Z. Zeng, Z. Yan, and T. Huang, "Sparse fully convolutional network for face labeling," *Neurocomputing*, vol. 331, pp. 465–472, Feb. 2019.
[27] S. Wen, M. Dong, Y. Yang, P. Zhou, T. Huang, and Y. Chen, "End-to-end detection-segmentation system for face labeling," *IEEE Trans. Emerg. Topics Comput. Intell.*, early access, Nov. 6, 2019, doi: 10.1109/TETCI.2019.2947319.

YIWEI CHEN was born in Fujian, China, in 1987. He received the B.S. degree from Nanjing University, in 2010, and the Ph.D. degree from the University of Chinese Academy of Sciences, in 2015. He was Postdoctoral Researcher with the University of Tsukuba, from 2015 to 2017, and with the University of Murcia, from 2018 to 2019. Since 2019, he has been working with the Suzhou Institute of Biomedical Engineering and Technology Chinese Academy of Sciences as an Associate Professor.

YI HE was born in Sichuan, China, in 1984. He received the B.S. degree in automation from the University of Science and Technology of China, in 2008, and the Ph.D. degree in measurement technology and instrument from the University of Chinese Academy of Sciences, in 2013. From 2013 to 2015, he was a Research Assistant with The Key Laboratory on Adaptive Optics, Chinese Academy of Sciences, Chengdu, China, where he has been an Associate Professor, since 2016. He is the author of more than 40 articles and more than 40 inventions. His research interests include biophotonics, biomedical imaging, confocal scanning imaging, optical coherence tomography imaging, and optical wavefront engineering for human eyes high-resolution imaging.

JING WANG was born in Kunming, Yunnan, China, in 1995. She received the B.S. degree in biomedical engineering from Beijing Jiaotong University, Beijing, in 2017. She is currently pursuing the master's degree in biomedical engineering with the University of Science and Technology of China, Hefei. Her research interests include image processing and machine learning-based retinal disease automatic diagnosis and treatment systems.

WANYUE LI was born in Xinjiang, China, in 1993. She received the B.S. degree from Xidian University, Xi'an, in 2016. She is currently pursuing the Ph.D. degree with the University of Science and Technology of China. She is also doing her research work with the Suzhou Institute of Biomedical Engineering and Technology Chinese Academy of Sciences. Her research interests include biomedical optical imaging and image processing techniques. Furthermore, she is specializing in the application of deep learning in medical image and optical image reconstruction.

LINA XING was born in Henan, China, in 1985. She received the B.S. and M.S. degrees from the College of Mechanical engineering, Chongqing University, in 2007 and 2010, respectively. From 2010 to 2012, she was a Research Trainee with the Changchun Institute of Optics, Fine Mechanics and Physics. From 2012 to 2017, she has been a Research Assistant with Changchun Institute of Optics, Fine Mechanics and Physics. Since 2017, she has been a Research Assistant with the Key Medical Optics Laboratory of Jiangsu Province, Suzhou Institute of Biomedical Engineering and Technology. Her research interests include optical machine structure design and optical coherence tomography research.

FENG GAO was born in Jiangxi, China, in 1991. He received the B.S. and M.S. degrees from the College of Optoelectronic Information, University of Electronic Science and Technology of China, in 2013 and 2016, respectively. From 2016 to 2018, he was a Research Trainee with the Key Medical Optics Laboratory of Jiangsu Province, Suzhou Institute of Biomedical Engineering and Technology. Since 2019, he has been a Research Assistant. His research interests include optical coherence tomography imaging and confocal ophthalmoscope research.

GUOHUA SHI was born in Zhejiang, China, in 1981. He received the B.S. degree from the Department of Optoelectronic Information Engineering, Zhejiang University, Hangzhou, China, in 2003, and the Ph.D. degree in optical engineering from the Institute of Optics and Electronics, Chinese Academy of Sciences. He is currently a Professor, the Ph.D. Advisor, the Director of the Medical Optics Technology Laboratory, the Vice Director of the Key Medical Optics Laboratory of Jiangsu Province, Suzhou Institute of Biomedical Engineering and Technology, Chinese Academy of Sciences. His research interests include the in vivo optical imaging and detecting method, as well as developing and industrializing the corresponding optical medical instruments.